THE BELL SYSTEM TECHNICAL JOURNAL
Vol. 54, No. 4, April 1975
Printed in U.S.A.

Line-of-Sight Paths Over Random Terrain

By E. N. GILBERT

(Manuscript received September 5, 1974)

Line-of-sight paths are important as VHF radio channels. In a mobile radio system, for example, the landscape determines the communication possibilities in a complicated way. This paper analyzes a simple model of rough terrain to relate statistical terrain properties to line-of-sight paths. The model is constructed from conical hills, all the same height, distributed at random over the surface of a spherical earth.

The parameters of the model are the earth's radius a, the density σ of hills, and the grade g of the hills. Although a simpler planar model is obtained by letting $a \to \infty$, a finite spherical earth is needed for most questions. Assuming that a base station is located at the peak of a hill, the most interesting line-of-sight paths are those from a typical hilltop. A large number of statistics of these paths are then derived, usually as simple functions of a, σ, and g. These include properties of paths to other peaks, to the horizon, and to random points on the ground.

I. INTRODUCTION

Very-high frequency radio propagation is often said to resemble optical propagation. A line-of-sight path provides a good radio channel; a path blocked by the terrain does not. With the aid of a topographic map, one can determine whether a path Q_1Q_2 is a line-of-sight path. Essentially, one must plot the ground elevation profile along the path to see whether the ground intersects the straight line segment Q_1Q_2. This calculation must include the effect of the earth's curvature. Atmospheric refraction is also accounted for by changing the earth's radius to a fictitious value.

Having done the calculation for one path Q_1, Q_2, we learn little about other paths. The region covered by a transmitter at Q_1, i.e., the set of points Q visible from Q_1, would be found by plotting ground elevation profiles along views from Q_1 at every possible azimuth angle. This region might represent the coverage of a TV station or of a base station in a mobile telephone system.

This paper analyzes a statistical model to give insight into the way coverage regions depend on properties of the terrain. The parameters

of the model are the radius a of the earth, a density σ of mountains (or hills) per unit area, and a grade (slope) g of these mountains. Many statistical properties of terrain and paths are then derived as functions of a, σ, g. These properties are means, or in some cases distribution functions, of the random variables that appear in the INDEX. Line-of-sight paths from a typical mountain peak receive special attention because a peak is the most likely site for a base station. Although the exact formulas contain integrals with unwieldy trigonometric integrands, most of these formulas may be replaced by simple expressions, to a very good approximation. The expected area visible from a peak and the expected number of peaks visible from a random point on the ground are more complicated quantities, leading to integrals that are evaluated numerically.

INDEX

Altitude—eqs. (6), (7), (8), Table I, Fig. 6.
Area blocking—eqs. (12), (17) to (20), (23), Table III.
  Visible—eq. (43), Table VII.
  Within horizon—eq. (35).
Number of peaks visible:
  From a peak—eq. (26), Table V.
  From a point on the ground—eq. (37).
Range from a peak:
  To furthest visible peak—eq. (31), Table V.
  To horizon—eqs. (33), (34), Table VI.
  To random visible peak—eqs. (25) to (29), Table IV.
  To random visible point on ground—eqs. (39) to (42), Fig. 15.
Slope—Table II.

The earth's radius a is an important parameter of the model. Although a simpler planar model is obtained by letting $a \to \infty$, the planar model is inadequate for most statistics of interest.

With a and σ fixed, the terrain becomes rougher as g increases. As a rule, the model predicts more long line-of-sight paths and larger expected visible area for rougher terrains. However, in mobile radio these long paths are more important as sources of interference than as useful channels.

II. THE MODEL

The terrain model will use conical mountains distributed at random in a Poisson pattern over the surface of the earth. Begin with a sphere of radius a miles (a may be the true radius of the earth, or something larger if atmospheric refraction effects are to be taken into account).

Place points at random on the surface S of this sphere using a Poisson process with density σ points per square mile. Each Poisson point will represent a mountain peak, and so the sphere of radius a will be called the *peak sphere.*

Each Poisson point P will be associated with a mountain-shaped subset $M(P)$ of the interior of the peak sphere. The subsets $M(P_1)$, $M(P_2)$, $\cdots$ for the various peaks will overlap. Take the union of all the subsets $M(P)$ to represent the earth.

The simplest shape for $M(P)$ is the cone consisting of all rays from P making angle $<\theta$ with the inward-pointing normal to S. This cone has to be truncated to keep it from extending beyond the peak sphere in the direction antipodal to P. The surface of the cone is tangent to an *inner sphere,* concentric with the peak sphere and having radius $a \sin \theta$. Take $M(P)$ to be the inner sphere plus the part of the cone that lies between P and the inner sphere. Figure 1 shows $M(P)$ shaded.

With this construction, the terrain consists of conical mountains, all having the same height and the same grade $g = \cot \theta$. There may also be flat places where the earth's surface coincides with the inner sphere. A flat spot occurs at any point that lies further than $(\frac{1}{2}\pi - \theta)$ radians away from all Poisson points. Flat spots are rare, except when the parameters σ, θ are chosen to produce widely separated mountains having very gentle slope.

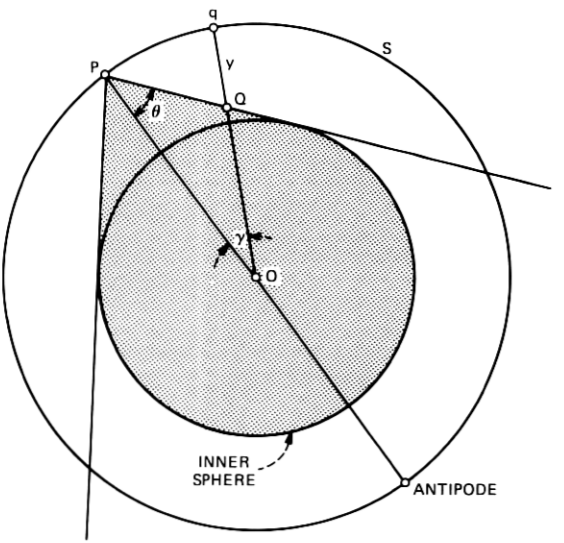

Fig. 1—Construction of $M(P)$.

Figure 2 is an elevation contour map for a typical random terrain. Some unrealistic features of the model are evident. The conically shaped mountains have circular contour lines. The peaks are distributed chaotically instead of being arranged in rows (mountain ranges).

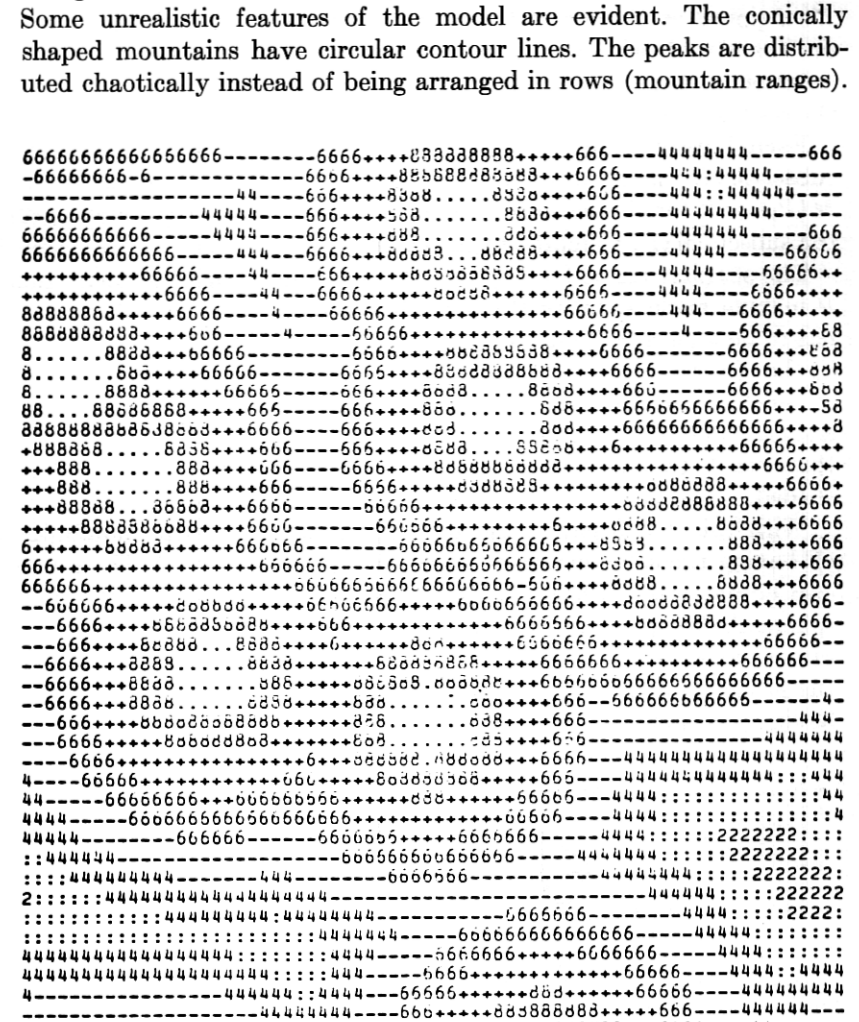

Fig. 2—Contour map. The symbols · 8 + 6 − 4 : 2 denote altitude levels ordered from the peak sphere downward.

Figure 3 is a plane cross section through the earth in the same model. This figure is more interesting for the present problem because the existence of a clear line-of-sight path between two points depends only on the shape of such a profile. Note that the elevation curve in Fig. 3 is composed of convex arcs (hyperbolas) that join in the valleys between mountains. But, at least, the maxima in Fig. 3 have different heights. Figure 4 shows random terrain as seen from one of the peaks looking out toward the horizon. The nearest and furthest peaks shown have ranges of 6 and 150 miles. The parameters were picked to match a particular portion of the Alps for which a panoramic photograph was also available. The deficiencies of the model are less evident in this figure. The curvature of the earth makes it less obvious that all peaks have the same height.

In real terrain, it is sometimes possible to see part of a mountain even though the mountain's peak is obscured from view. That cannot happen in this model, as will now be proved. Suppose that the view of a peak P_1 is blocked when the eye is at E. Then the line segment P_1E contains a blocking point B_2 belonging to another mountain $M(P_2)$. Now consider any other point P of $M(P_1)$. P must lie on some line segment P_1I, where I belongs to the inner sphere. Figure 5 shows the triangle EP_1I. The segments EP and B_2I cross at some point B in the triangle. B belongs to the convex set $M(P_2)$ because B_2 and I belong. Then B is a point of $M(P_2)$ blocking the view of P.

By making $a \to \infty$, one obtains a *planar model* of random topography. The peak sphere S becomes a peak plane. At a point Q, the land surface lies below the peak plane a distance

$$y = g \operatorname*{Min}_i \|P_i - Q\|, \tag{1}$$

where the minimization is over all Poisson points P_i. Replacing S by a plane simplifies the analysis considerably but, unfortunately, it produces a much less realistic model. If Fig. 4 has been drawn for a planar model, every peak P_i would have been visible. Even worse, Section VIII shows that the expected area visible from a peak would be infinite. For that reason, the extra complication of a spherical earth is really necessary for some questions about line-of-sight paths.

III. PARAMETER ESTIMATION

The two parameters σ, $g = \cot\theta$ can be chosen to fit the model to terrain measurements. One might estimate the density σ by counting peaks. A difficulty is that one must then decide how big a hill must be to be counted. Surely every bump on the landscape ought not to count as a peak. This decision is avoided by using statistical properties of the point Q lying below a random point q on the peak sphere. The

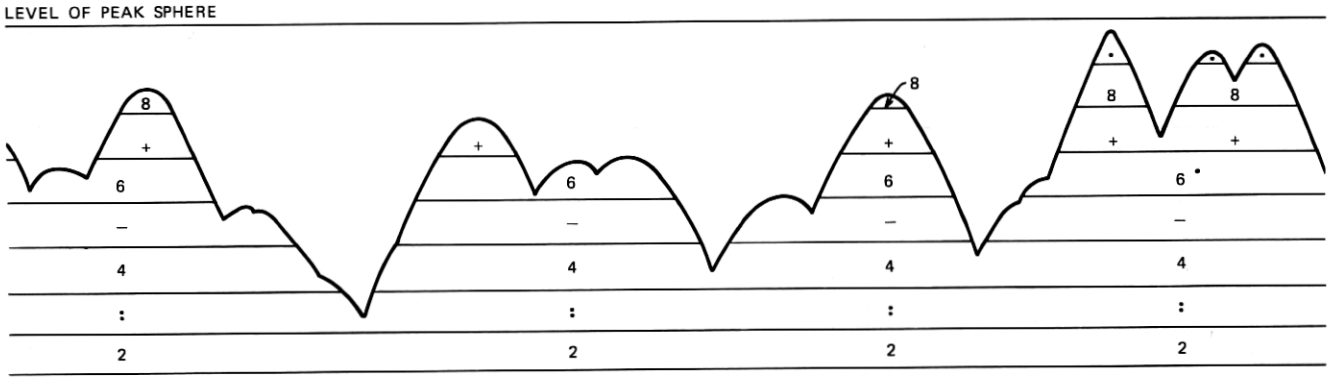

Fig. 3—Cross-section view.

Fig. 4—View of horizon from a peak.

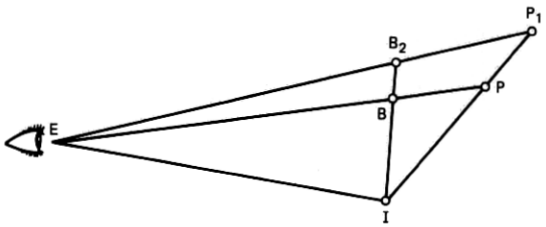

Fig. 5—$M(P_2)$ blocks all of $M(P_1)$ from view if it blocks P_1.

altitude and slope of the terrain at Q are two useful random variables. Both depend on the angle $\gamma = < POQ$ from Q to the nearest peak P (see Fig. 1). Since a circular cap of angle γ_0 on the peak sphere has area $2\pi a^2(1 - \cos \gamma_0)$, the distribution function for $<POQ$ can be written immediately,

$$\text{Prob } (\gamma \leqq \gamma_0) = 1 - \exp [- 2\pi a^2 \sigma (1 - \cos \gamma_0)]. \tag{2}$$

There is no natural sea level in the model, and so it will be convenient to specify the altitude at Q by giving the *depth* y, measured from S down to the land. If $\gamma \geqq \frac{1}{2}\pi - \theta$, then ground level coincides with the inner sphere, i.e.,

$$y = a(1 - \sin \theta), \qquad \gamma \geqq \tfrac{1}{2}\pi - \theta. \tag{3}$$

For smaller angles γ,

$$y = a[1 - \sin \theta / \sin (\gamma + \theta)], \qquad 0 \leqq \gamma < \tfrac{1}{2}\pi - \theta, \tag{4}$$

as is clear from Fig. 1. These formulas, together with the distribution (2) for γ, determine the depth distribution,

$$\begin{aligned} \text{Prob } \{y \leqq a[1 - \sin \theta / \sin (\gamma + \theta)]\} \\ = 1 - \exp [-2\pi a^2 \sigma (1 - \cos \gamma)], \qquad 0 \leqq \gamma < \tfrac{1}{2}\pi - \theta \\ \text{Prob } \{y \leqq a(1 - \sin \theta)\} = 1. \end{aligned} \tag{5}$$

Although one can easily tabulate the distribution function for y by substituting numerical values of γ into (5), the distribution function is easier to visualize in a limiting case. Since a is a large radius, let $a \to \infty$ in (5). As one might expect, the formulas tend toward the depth distribution function in the planar model,

$$\text{Prob } \{y \leqq Y\} = 1 - \exp [-\sigma \pi (Y/g)^2]. \tag{6}$$

In this limit, σ and g enter the distribution only via a single length parameter $\sigma^{-\frac{1}{2}} g$, which is an index of altitude variability. Thus, altitude distribution data alone cannot be expected to supply good estimates of

both g and σ. Some simpler statistics are the median,

$$\begin{aligned}\text{Median } (y) &= (\pi^{-1} \log_e 2g^2/\sigma)^{\frac{1}{2}} \\ &= 0.4697\sigma^{-\frac{1}{2}}g,\end{aligned}$$

and the moments,

$$E(y^k) = \Gamma(1 + \tfrac{1}{2}k)(g^2/\pi\sigma)^{k/2}.$$

Particularly, the mean is

$$\bar{y} = E(y) = \tfrac{1}{2}\sigma^{-\frac{1}{2}}g \tag{7}$$

and the standard deviation is

$$[\text{Var } (y)]^{\frac{1}{2}} = [(\pi^{-1} - 2^{-2})g^2/\sigma]^{\frac{1}{2}} = 0.2683\sigma^{-\frac{1}{2}}g. \tag{8}$$

It is also possible to obtain (6) as an exact result for a spherical model in which the shape of the mountains is only approximately conical. That entails a new choice of the set $M(P)$ in Fig. 1. Define the new shape so that the depth becomes

$$y = 2ga \sin \tfrac{1}{2}\gamma, \tag{9}$$

where again γ is the angle to the peak. At P, $M(P)$ comes to a point approximating a cone of slope g. At the antipode to P, $M(P)$ has depth $2ga$; then this model requires $g < \frac{1}{2}$. Now the depth distribution for all γ is again given by (5) but with the left-hand side replaced by Prob $\{y \leqq 2ga \sin \frac{1}{2}\gamma\}$. But that is (6), exactly.

For many values of g and σ, the planar approximation (6) to the depth distribution (5) is very good. For example, Table I compares the planar approximation with some distributions having $a = 3959$ mi, the earth's radius. In the table, the cones have grades $g = 0.05$, 0.1, and 0.2 and the density σ is adjusted to fix the standard deviation in (8) at 528 ft (0.1 mi). Table I gives percentiles of the distribution as

Table I — Altitude percentiles (in feet)

	Spherical Model			Planar
$g =$ $\sigma =$	0.05 0.0171	0.1 0.0683	0.2 0.2732	$\sigma/g^2 = 6.831$
0.1%	−1899	−1964	−1980	−1986
1%	−1378	−1421	−1432	−1436
10%	−691	−712	−717	−719
25%	−315	−327	−331	−332
50%	70	63	62	61
75%	402	400	399	399
90%	642	641	640	640
99%	896	896	896	896

altitudes measured upward from a common level, corresponding to the depth $\bar{y}$ in (7).

Figure 6 is an altitude distribution for northern New Jersey. It was obtained from a topographic map by reading altitudes at 52 points, 10 km apart in a rectangular grid covering latitudes 40°30′ to 41° and longitudes west of 74°. The altitudes ranged from 0 to 1100 ft. Data for parts of New Jersey further south were not used; the topography of New Jersey is too variable for both north and south to be well represented by a single simple model. The planar model fits the observed points well, except at low altitudes. As an alternative, use the spherical model with $a = 3959$ mi. By taking $g = 0.011$, one obtains a maximum depth (3) near 1100 ft, so that low altitudes can be regarded as occurring on the inner sphere. Then σ remains as a parameter to adjust for a good fit.

The parameter $g = \cot\theta$ is the grade at mountain peaks. At the random point Q, at angle γ away from a peak in Fig. 1, the grade is smaller because the normal to the conical surface makes an angle $\frac{1}{2}\pi - \theta - \gamma$ with the vertical direction OQ. Thus, the grade at Q is

$$g' = \begin{cases} \cot(\theta + \gamma) = (g - \tan\gamma)/(1 + g\tan\gamma), & \text{if } \theta + \gamma \leqq \frac{1}{2}\pi \\ 0 \quad \text{otherwise.} \end{cases}$$

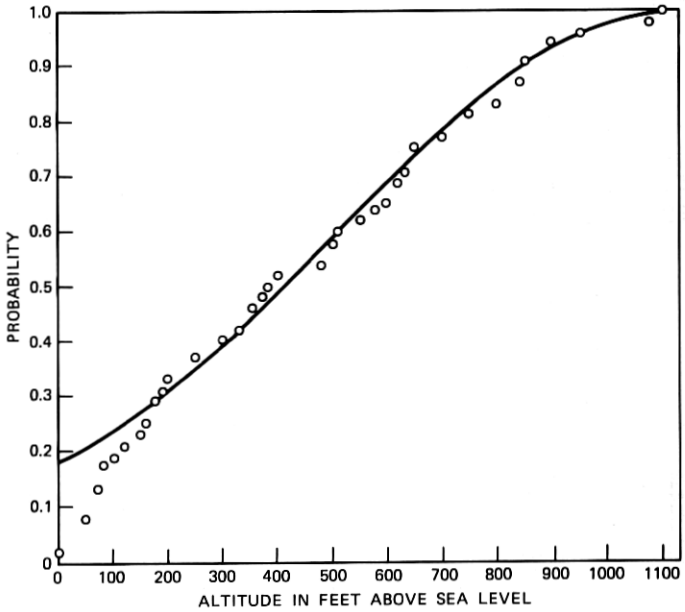

Fig. 6—Altitude distribution for northern New Jersey. Curve is for planar model with peak sphere at 1130-ft altitude and $[\text{Var}\ (y)]^{\frac{1}{2}} = 400$ ft.

Table II — Percentiles of G/g

g =	small	0.1	0.2	0.5
0%	−1.0000	−1.0000	−1.0000	−1.0000
1%	−0.9995	−0.9995	−0.9995	−0.9994
10%	−0.9510	−0.9506	−0.9492	−0.9399
25%	−0.7070	−0.7053	−0.7001	−0.6667
50%	0	0	0	0
75%	0.7070	0.7053	0.7001	0.6667
90%	0.9510	0.9506	0.9492	0.9399
99%	0.9995	0.9995	0.9995	0.9994
100%	1.0000	1.0000	1.0000	1.0000

The grade 0 occurs on the inner sphere. This result, together with (2), determines the distribution of the grade g'. In most cases, the grade g' has high probability of being close to g; one should not expect this distribution to fit observed grade data well.

At q, one might move in a random direction and ask for the slope G along the random path through Q. The slope, which depends on the angle φ between the path direction and the uphill direction, lies in the range $-g' \leqq G \leqq g'$. With some simple geometry, one finds

$$G = g' \cos \varphi/(1 + g'^2 \sin^2 \varphi)^{\frac{1}{2}}.$$

By using the known distribution for g' and assuming a flat distribution for φ, one can obtain a distribution function for G. This would be the distribution of the slopes G seen in cross sections like Fig. 3. A simple distribution is obtained only in the planar model limit, for which $g' = g = \cot \theta$ identically:

$$\text{Prob } \{G \leqq \tan \chi\} = 1 - \pi^{-1} \arccos \{\sin \chi/\cos \theta\}.$$

Table II gives the slope distribution in the planar model for several values of g. In the limit of small g, the distribution function for G/g tends to $1 - \pi^{-1} \arccos G/g$.

IV. BLOCKING REGIONS

Suppose two points Q_1, Q_2 are given, representing the positions of two antennas. In general, Q_1, Q_2 can lie anywhere above the inner sphere. A clear line-of-sight path exists between Q_1 and Q_2 as long as the straight-line segment Q_1Q_2 does not intersect any of the sets $M(P_i)$. The *blocking region* for Q_1, Q_2 is the (open) set of points P on S such that Q_1Q_2 intersects $M(P)$. The area of the blocking region enters into the probability that a line-of-sight path Q_1Q_2 exists. The advantage of the conical mountains $M(P)$ is that blocking regions assume simple shapes.

The simplest blocking region is one for a pair of points Q_1, Q_2 both on S. If the line Q_1Q_2 intersects the inner sphere, all $M(P_i)$ block the path. The blocking region then consists of the entire sphere S. If Q_1Q_2 misses the inner sphere, then blocking occurs at a point Q on the path Q_1Q_2 if a peak P_i lies too close to Q. If the depth of Q is y, then (4) gives the angle γ to peaks P such that Q lies on the surface of $M(P)$. Then blocking occurs at Q if a circular cap of angular radius γ contains a peak. The pole of this cap is the radial projection q of Q onto S. The blocking region for the path Q_1Q_2 is the union of all the blocking caps for points Q on the path. These caps are largest midway between Q_1 and Q_2, shrinking to points at Q_1 and Q_2. Then the blocking region is lens-shaped, as in Fig. 7.

Figure 7 shows two arcs K, K' which form the boundary of the blocking region. The argument that follows shows that K, K' are actually arcs of circles. Figure 8 is another view of the peak sphere projected directly along the line Q_1, Q_2. Two planes, π and π', can be drawn through Q_1, Q_2 and tangent to the inner sphere, say at C and C'. These planes project to lines in Fig. 8. The planes π and π' intersect S in two circles, centered at C and C' and both passing through Q_1 and Q_2. Since $M(P)$ is the convex hull of P and the inner sphere, π is a supporting plane of $M(P)$ as long as P lies below π (i.e., in the half-space containing the inner sphere). Then $M(P)$ does not block the path Q_1Q_2 if P lies below π, or below π'. The part of S lying above both π and π' appears shaded in Fig. 8. Suppose P belongs to the shaded region. Project the triangle $C'PC$, a subset of $M(P)$, onto the plane of Fig. 8. The path Q_1Q_2 projects to a point lying inside this projected triangle. Then Q_1Q_2, a chord of S, must intersect the triangle $C'PC$.

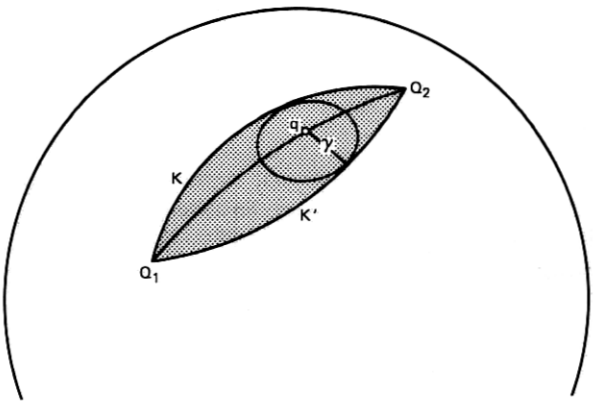

Fig. 7—Blocking region for two points Q_1, Q_2 on the peak sphere.

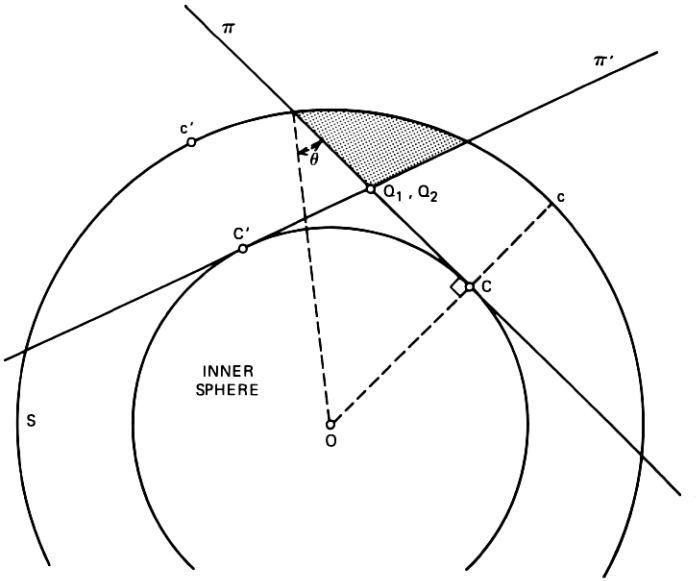

Fig. 8—Another view of the blocking region.

The point of intersection is a point of $M(P)$, which blocks the path. Thus, the shaded region, bounded by arcs of the circles $S \cap \pi$, $S \cap \pi'$, is the blocking region for Q_1Q_2.

The area $A(Q_1, Q_2)$ of the blocking region in Fig. 7 will now be expressed as a function of the angle $2\rho = \angle Q_1OQ_2$. Project the centers C, C' in Fig. 8 radially out to c, c' on S. Figure 9 is another view of S showing c, c' as the poles of two circular caps bounded by $S \cap \pi$ and $S \cap \pi'$. The angular radius of both caps is $\frac{1}{2}\pi - \theta$, as is clear from Fig. 8. The chord Q_1Q_2 subtends some angle $2\alpha = \angle Q_1cQ_2$ at c. Using the spherical sine law in the right triangle Q_1, c, $\frac{1}{2}(Q_1 + Q_2)$, one may determine α from

$$\sin \alpha = \sin \rho / \cos \theta. \tag{10}$$

The cap with pole c has area $2\pi a^2(1 - \sin \theta)$ and the sector included within angle 2α has area

$$A_s = 2\alpha a^2(1 - \sin \theta).$$

Also, the triangle Q_1cQ_2 has area

$$A_T = (2\alpha + 2\beta - \pi)a^2,$$

where $\beta = Q_1Q_2C_1 = Q_2Q_1c$. The sine law may be applied to triangle Q_1cQ_2 to find β

$$\sin \beta = \cos \theta \sin 2\alpha / \sin 2\rho. \tag{11}$$

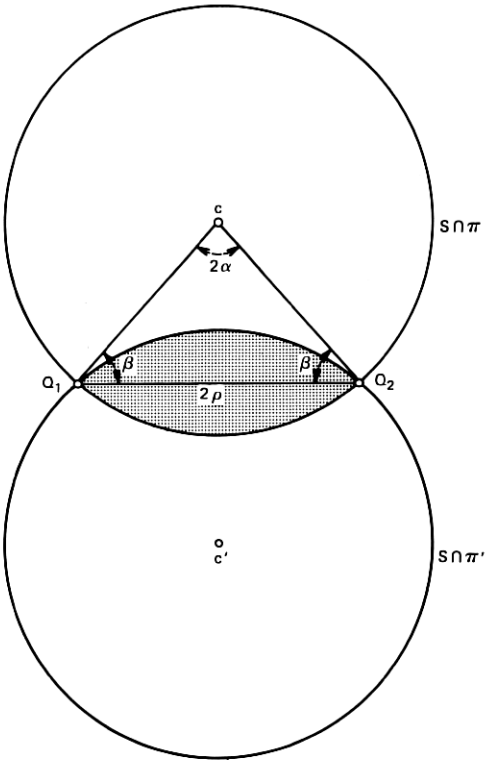

Fig. 9—Angles used in deriving area A of blocking region.

The difference $A_S - A_T$ is $\frac{1}{2}A(Q_1, Q_2)$. Thus,

$$A(Q_1, Q_2) = a^2(2\pi - 4\beta - 4\alpha \sin \theta), \tag{12}$$

where (10), (11) give α, β.

The blocking region is more complicated if Q_1, Q_2 or both are not on S. As in Fig. 7, each point Q on Q_1Q_2 is blocked by peaks lying in a circular cap of radius γ given by (4); the blocking region is the union of these caps. Let Q_1', Q_2' be the points where the extended line Q_1Q_2 meets S. The blocking region for Q_1Q_2 is a subset of the blocking region for $Q_1'Q_2'$. As shown in Fig. 10, the blocking region consists of the caps for blocking at Q_1 and Q_2 plus the part of the blocking region for $Q_1'Q_2'$ that lies between these caps. The centers of the two end caps are the points q_1, q_2 obtained by projecting Q_1, Q_2 radially onto S.

The two end caps have a special role in the blocking. Normally, Q_1, Q_2 are known to lie above ground, and so the two end caps are known to contain no peaks. If the ground levels below q_1, q_2 are known, then peaks P_1, P_2 must exist somewhere at the appropriate angles γ_1,

γ_2 away from q_1, q_2. In Fig. 10, Q_1, Q_2 are assumed to be at ground level; then P_1, P_2 lie on the boundaries of the end caps. The mountains $M(P_1)$, $M(P_2)$ on which Q_1, Q_2 lie can themselves block the path Q_1Q_2. Thus, in Fig. 10, P_2 blocks the path because it lies in the blocking region. To compute the conditional blocking probability for the configuration in Fig. 10, one must know both the area of the part of the blocking region that lies outside the end caps and also angles φ_1, φ_2 that limit where P_1, P_2 can lie to cause blocking. In the applications that follow, it will suffice to let Q_1 lie at a peak $Q_1 = P_1$ and let Q_2 be a point at ground level. That simplifies Fig. 10 to Fig. 11.

Let $z_2 = \angle P_1 0 q_2$, the angular distance along the arc P_1q_2. The depth at Q_2 determines the angle γ_2 of the end cap. The sides of the spherical triangle P_1q_2c are now known, and so its angles $\beta = \angle q_2P_1c$, $\zeta_2 = \angle q_2cP_1$, $\pi - \varphi_2 = \angle P_1q_2c$ are determined. One finds

$$\tan \tfrac{1}{2}\varphi_2 = \left\{ \frac{1 - \cos(z_2 - \gamma_2) + g \sin(z_2 - \gamma_2)}{g \sin(z_2 + \gamma_2) - 1 + \cos(z_2 + \gamma_2)} \right\}^{\frac{1}{2}} \tag{13}$$

$$\sin \beta = \sin \varphi_2 \cos(\theta + \gamma_2)/\cos \theta \tag{14}$$

$$\sin \zeta_2 = \sin \varphi_2 \sin z_2/\cos \theta. \tag{15}$$

The blocking area is twice the area of the half of the blocking region above the line P_1Q_2' in Fig. 11. That half can be obtained as a sum of two parts. One part is a sector of angle $\pi - \varphi_2$ from the end cap; its area is $(\pi - \varphi_2)(1 - \cos \gamma_2)a^2$. The other part is obtained by removing

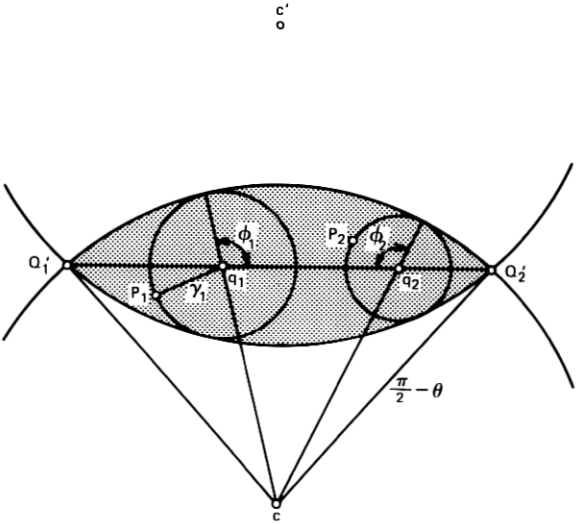

Fig. 10—Blocking region for points Q_1, Q_2 which are not peaks.

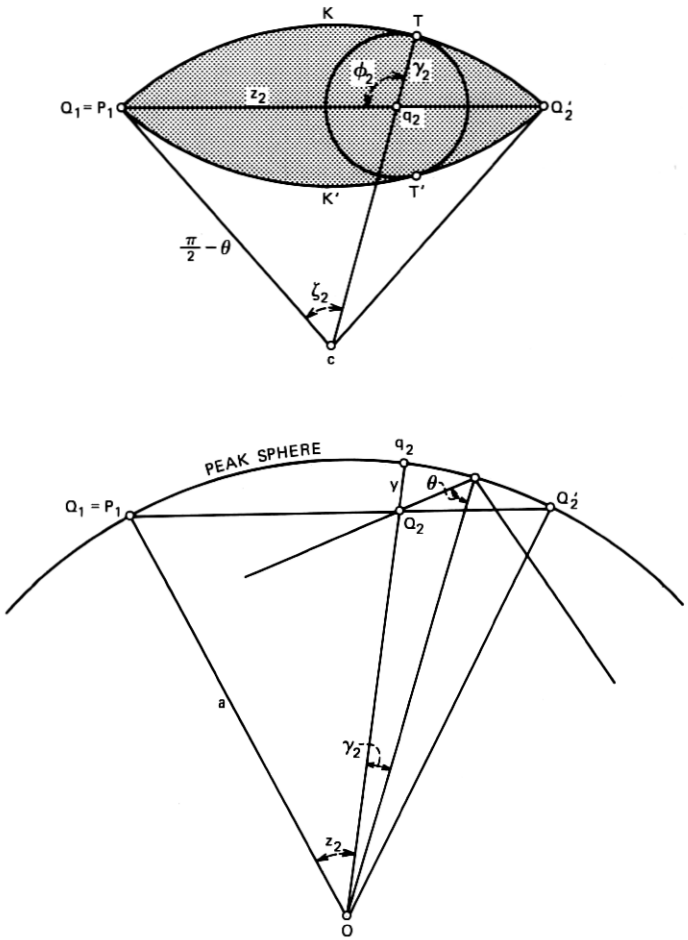

Fig. 11—Blocking region for $Q_1 = P$, a peak, Q_2 not a peak.

the triangle P_1q_2c of area $(\beta + \zeta_2 - \varphi_2)a^2$ from a sector centered at c. The sector has area $\zeta_2(1 - \sin\theta)a^2$. These areas may be combined to express the area of the blocking region in the form

$$A(Q_1, Q_2) = A_0 + A_2,$$

where

$$A_2 = 2\pi(1 - \cos\gamma_2)a^2 \tag{16}$$

and

$$A_0 = (2\varphi_2 \cos\gamma_2 - 2\beta - 2\zeta_2 \sin\theta)a^2. \tag{17}$$

A_2 is the area of the end cap and A_0 is the area of the remainder of the blocking region.

Although the blocking area $A(Q_1, Q_2)$ for the general situation of Fig. 9 will not be needed, it can be obtained in the form

$$A(Q_1, Q_2) = A(Q_1', Q_2) + A(Q_1, Q_2') - A(Q_1', Q_2'). \tag{18}$$

Note that formulas like (16) and (17) give $A(Q_1', Q_2)$, $A(Q_1, Q_2')$ while (10), (11), and (12) give $A(Q_1', Q_2')$. Likewise, with a change of subscripts, (13) gives φ_1 as well as φ_2.

These formulas can now be used to obtain the *path probability* $p(Q_1, Q_2)$, the conditional probability that a clear line-of-sight path exists between given points Q_1, Q_2. When Q_1, Q_2 are on S, as in Fig. 7, $p(Q_1, Q_2)$ is just the probability that the shaded region of area $A(Q_1, Q_2)$ contains no peaks. Then

$$p(Q_1, Q_2) = \exp\left[-\sigma A(Q_1, Q_2)\right], \tag{19}$$

with $A(Q_1, Q_2)$ given by (12).

The situation in Fig. 11 is more complicated. $Q_1 = P_1$, a peak, and Q_2 is supposed to lie on the ground. Then the cap of area A_2 is known to be empty. Two conditions must hold if the entire blocking region is to be empty. One is that the peak P_2 of the mountain on which Q_2 lies causes no blocking. Since P_2 is equally likely to be anywhere on the boundary of the cap around Q_2, there is probability $1 - \varphi_2/\pi$ that P_2 does not block the path. The second condition is that the remainder of area A_0 of the blocking region is empty. Then

$$p(Q_1, Q_2) = (1 - \varphi_2/\pi) \exp(-\sigma A_0), \tag{20}$$

where (13) and (17) give φ_2 and A_0. Formula (20) applies as long as $\gamma_2 < z_2$. It is also possible to have $\gamma_2 = z_2$. In that case, Q_2 lies on the mountain $M(P_1)$; the path in question runs from the peak $Q_1 = P_1$ to Q_2 along the surface of the cone $M(P_1)$. Whether or not such a path is to be considered blocked is a matter of definition. Here $M(P_1)$ is regarded as an open set so that the path is not blocked. As $\gamma_2 \to z_2$, one finds $\varphi_2 \to 0$ and $A_0 \to 0$ so that $p(Q_1, Q_2) \to 1$, i.e., (20) continues to give the correct probability in the limit.

Another limiting situation, $\gamma_2 \to 0$, illustrates an important distinction between Figs. 11 and 7. In the limit $A_2 \to 0$ and A_0 becomes the area of a lens-shaped region, such as shown in Fig. 7. Then the exponential factor in (20) becomes the path probability (19) for the two peaks $Q_1 (= P_1)$, and $\lim Q_2$. However, (20) contains an extra factor $(1 - \varphi_2/\pi)$ which approaches $\frac{1}{2}$, not 1. This disagreement between (19) and (20) is explained as follows. From a point Q_2 near a peak P_2, one can look over a 180-degree view; the mountain $M(P_2)$ blocks the other 180 degrees. Then the factor $\frac{1}{2}$ in (20) is needed to account for possible blocking by $M(P_2)$. But exactly at the peak

$Q_2 = P_2$, the mountain $M(P_2)$ no longer interferes in any direction. Then no factor $\frac{1}{2}$ is needed in (19). The discontinuity in $p(Q_1, Q_2)$ as $Q_2 \to P_2$ could be avoided by assuming that the antenna location Q_2 lies at some known positive height h above ground.

V. PATHS BETWEEN PEAKS

The simplest blocking regions were for paths Q_1Q_2 with both end points on mountain peaks. The path probability $p(Q_1, Q_2)$ in (19) can now be used to derive some interesting properties of peak-to-peak paths. In this section, Q_1 will be a given peak P_1. Q_2 will be another peak selected at random. An element of area $dA(Q_2)$ on the peak sphere S has probability $\sigma dA(Q_2)$ of containing a peak Q_2. Then $\sigma p(Q_1, Q_2)dA(Q_2)$ is the probability that the element contains a peak Q_2 which is visible from Q_1.

Let $d(Q_1, Q_2)$ denote great circle distance between Q_1 and Q_2. Let $\Sigma_k(d)$ denote the random variable which is the sum

$$\Sigma_k(d) = \sum_i d(Q_1, P_i)^k \tag{21}$$

of kth powers of distances from Q_1 to all other visible peaks P_i lying within distance $d[d(Q_1, P_i) \leqq d]$. The element $dA(Q_2)$ contributes a term $d(Q_1, Q_2)^k$ to $\Sigma_k(d)$ with probability $\sigma p(Q_1, Q_2)dA(Q_2)$. Thus, the expected value of $\Sigma_k(d)$ is

$$E[\Sigma_k(d)] = \sigma \int\int d(Q_1, Q_2)^k p(Q_1, Q_2)dA(Q_2), \tag{22}$$

where the integral extends over all points Q_2 in the cap $d(Q_1, Q_2) \leqq d$. Another random variable Σ_k is a sum like (21) extended over all visible peaks, at any distance from Q_1. The mean $E(\Sigma_k)$ is an integral (22) over the entire sphere. Evaluating (22) will give the mean number

Table III — Blocking area $A(Q_1, Q_2)$ in square miles, as given by exact and approximate formulas (12) and (23) with range $d(Q_1, Q_2) = 100$ miles

Grade g	Exact	Approximate
0.01263	7887.7	3333.1
0.02	2430.9	2104.9
0.05	857.6	842.0
0.1	423.2	421.0
0.2	210.2	210.5
0.5	84.1	84.2
1.0	42.0	42.1

of visible peaks $E(\Sigma_0)$ and other information about the distances to visible peaks. That could be done numerically, using (10), (11), (12), and (19). However, the approximation that follows simplifies the evaluation.

The approximation is one which holds when a is so large that angles 2ρ between visible peaks can be considered small. The planar model has $A(Q_1, Q_2) = 0$ and $p(Q_1, Q_2) = 1$, which is too rough to make sense in (22). Instead, the first nonzero term in a series for $A(Q_1, Q_2)$ in powers of ρ will be used. Expansion of the exact formulas (10), (11), and (12) is laborious but straightforward:

$$\begin{aligned} \alpha &= \rho(1 + g^2)^{\frac{1}{2}}/g + \rho^3(1 + g^2)^{\frac{1}{2}}/(6g^3) + 0(\rho^5) \\ \beta &= \tfrac{1}{2}\pi - \rho/g - (2g^2 + 1)\rho^3/(6g^3) + 0(\rho^5) \\ A(Q_1, Q_2) &= a^2(2\rho)^3/(6g) + 0(\rho^5). \\ &= r^3/(6ga) + \cdots, \end{aligned}$$

where $r = 2a\rho$ is the great circle distance $d(Q_1, Q_2)$.

For a simpler, more intuitive, derivation, one may find the size of the circle about a typical point q along the path Q_1, Q_2 in Fig. 7. If z is the great circle distance from Q_1 to q, then the ground level below q lies at depth y satisfying

$$(a - y) \cos (z - \tfrac{1}{2}r)/a = a \cos \tfrac{1}{2}r/a$$

or

$$y = z(r - z)/(2a) + \cdots.$$

The radius $a\gamma$ of the circle about q is approximately y/g, and the blocking area is approximately

$$\begin{aligned} A(Q_1, Q_2) &= \int_0^r a\gamma dz \\ &= \int_0^r z(r - z)dz/(2ag) \\ A(Q_1, Q_2) &= r^3/(6ga) + \cdots, \end{aligned} \tag{23}$$

as before.

From the form of the series used in deriving (23), one may predict that the rate of convergence is determined by the ratio ρ/g. Table III shows that (23) does give a better approximation for large g than for small. In Table III, $a = 3959$ mi; a large range, 100 mi, was used for a severe test of the approximation. At grades g smaller than 0.01263, a 100-mi path between peaks is blocked by the inner sphere. The small ρ/g condition is another way of requiring that the path Q_1Q_2 clears the inner sphere by a safe margin.

Now use the approximation (23) for $A(Q_1, Q_2)$ in (19) to evaluate the integral (22) for the expectation $[\Sigma_k(d)]$:

$$E[\Sigma_k(d)] = 2\pi\sigma \int_0^{d/(2a)} (2a\rho)^{k+1} \exp\{-4a^2\sigma\rho^3/3g\} 2ad\rho$$

$$E[\Sigma_k(d)] = (2\pi\sigma/3)D^{k+2} \int_0^{(d/D)^3} u^{(k-1)/3} \exp(-u)du, \qquad (24)$$

where

$$D = (6ag/\sigma)^{\frac{1}{3}}.$$

The integral in (24) may be expressed in terms of the incomplete gamma function,

$$E[\Sigma_k(d)] = (2\pi\sigma/3)D^{k+2}\{\Gamma[(k+2)/3] - \Gamma[(k+2)/3], (d/D)^3\},$$

or the χ^2 distribution function,

$$E[\Sigma_k(d)] = (2\pi\sigma/3)D^{k+2}\Gamma[(k+2)/3]P(\chi^2|\nu),$$

where

$$\chi^2 = 2(d/D)^3$$

and the number of degrees of freedom is

$$\nu = 2(k+2)/3.$$

Although the approximation (23) becomes poor at long ranges, the integrand is very small there. Thus, (24) can be expected to hold even for long ranges. In particular, the expectation $E(\Sigma_k)$, for visible peaks of all ranges, may be approximated by letting $d \to \infty$ in (24):

$$E(\Sigma_k) = (2\pi\sigma/3)D^{k+2}\Gamma[(k+2)/3]. \qquad (25)$$

For the special value $k = 0$, (25) gives the mean number of peaks visible from Q_1:

$$\begin{aligned} E(\Sigma_0) &= \pi\sigma D^2\Gamma(5/3) \\ &= 9.3645(a^2g^2\sigma)^{\frac{1}{3}} \\ &= 2344(g^2\sigma)^{\frac{1}{3}} \quad \text{if} \quad a = 3959 \text{ mi}. \end{aligned} \qquad (26)$$

Note, as predicted earlier, that the mean number of visible peaks tends to infinity in the limit of large a (planar model). When $k = 1$, (25) simplifies to

$$E(\Sigma_1) = 4\pi ag. \qquad (27)$$

As σ increases, (26) shows that the mean number of visible peaks increases, but (27) shows that the mean sum of distances to visible peaks remains unchanged. This indicates that visible peaks tend to be closer for large σ than for small. One way to define a range for a

"typical" peak is to form the ratio

$$\begin{aligned} D_1 &= E(\Sigma_1)/E(\Sigma_0) = D/\Gamma(2/3) \\ &= 0.738487D \\ &= 1.34190(ag/\sigma)^{\frac{1}{3}}. \end{aligned} \tag{28}$$

VI. RANGES BETWEEN PEAKS

One might ask for a probability distribution for the range d from a peak P_1 to a randomly chosen visible peak $P \neq P_1$. The random process for choosing a peak must be specified with care. Perhaps the most natural process would be this. Construct a random landscape and choose a peak P from the set of Σ_0 visible peaks, all peaks equally likely. Then ask for the probability that P is one of the $\Sigma_0(d)$ peaks within range d of P_1. Given a landscape, the conditional probability that P is within range is $\Sigma_0(d)/\Sigma_0$. Then the unconditioned probability is $E[\Sigma(d)/\Sigma_0]$. Unfortunately, the expectation is hard to obtain [there is also a question of giving an appropriate meaning to $\Sigma_0(d)/\Sigma_0$ when $\Sigma_0(d) = \Sigma_0 = 0$].

By using a different random process, one obtains a simpler distribution. Construct a trial random landscape and pick one of the peaks P at random, this time from the set of all peaks on the entire sphere S. P may not be visible. If not, discard that trial and construct a new landscape. Continue constructing landscapes and choosing peaks until the chosen point P is visible. Then ask for the probability $p(d)$ that P lies within range d.

To determine $p(d)$, note that the total number of peaks on the entire sphere has the Poisson distribution with mean $4\pi a^2\sigma$. The argument to follow assumes that this number is large, so that the number of peaks actually obtained is almost always very close to its mean value. Then the probability that P is visible is $E(\Sigma_0)/(4\pi a^2\sigma)$. If $q[\Sigma_0, \Sigma_0(d)]$ is the joint probability for Σ_0 and $\Sigma_0(d)$ in each trial, then $q[\Sigma_0, \Sigma_0(d)]\Sigma_0/(4\pi a^2\sigma)$ is the probability that a trial has Σ_0 visible peaks, $\Sigma_0(d)$ within range d, and that P is visible. The joint probability for the numbers Σ_0, $\Sigma_0(d)$ of the landscape, selected when P is visible, is $q'[\Sigma_0, \Sigma_0(d)] = q[\Sigma_0, \Sigma_0(d)]\Sigma_0/E(\Sigma_0)$. The probability that P lies within range d is obtained as a sum over $\Sigma_0(d)$ and Σ_0

$$\begin{aligned} p(d) &= \sum q'[\Sigma_0, \Sigma_0(d)]\Sigma_0(d)/\Sigma_0 \\ &= E[\Sigma_0(d)]/E(\Sigma_0) \\ p(d) &= 1 - \Gamma[2/3, (d/D)^3]/\Gamma(2/3), \end{aligned} \tag{29}$$

the last line following from (24).

It is clear from this derivation that the second random process tends to select random landscapes with larger Σ_0 than the landscapes

Table IV — Probability $p(d) = E(\Sigma_0(d))/E(\Sigma_0)$ that a randomly chosen visible peak lies within range d

d/D	Probability
0.25	0.06880
0.30211	0.1
0.48595	0.25
0.5	0.26361
0.72212	0.5
0.75	0.53050
1	0.77518
1.20507	0.9
1.32182	0.95
1.5	0.98440
1.55886	0.99
1.81350	0.999
2	0.99983

of the first process. However, Σ_0 may be expected to have a highly peaked distribution, in which case Σ_0 is nearly always close to $E(\Sigma_0)$. Then $q(\cdot, \cdot)$ and $q'(\cdot, \cdot)$ are nearly the same, and (29) is also a good approximation to the range distribution for the first random process.

Equation (29) provides numerical values for the range distribution in Table IV.

Another random variable of interest is the range to the furthest visible peak. Even the expectation of this maximum range is hard to derive. However, a simpler "typical" maximum range is the range d_m such that the expected number of visible peaks with ranges $d > d_m$ is just $\frac{1}{2}$. Then d_m satisfies

$$E(\Sigma_0) - E[\Sigma_0(d_m)] = \tfrac{1}{2}, \tag{30}$$

and (24) shows that

$$\int_{(d_m/D)^2}^{\infty} u^{-\frac{1}{2}} \exp(-u)du = 3/(4\pi\sigma D^2). \tag{31}$$

Table V — Mean number of visible peaks $E(\Sigma_0)$ and range d_m such that $E(\Sigma_0\text{-}\Sigma_0(d_m)) = \frac{1}{2}$

σD^2	$a^2g^2\sigma$	$E(\Sigma_0)$	d_m/D
3.11	0.84	8.8	1.30
5.69	5.12	16.1	1.40
11.3	40.1	32.1	1.50
24.5	409	69.5	1.60
58.4	5528	165.6	1.70
153.6	100572	435.5	1.80
450.5	2.54×10^6	1278	1.90
1477	8.95×10^7	4189	2.00
5447	4.49×10^9	15448	2.10

Table V gives numerical values of d_m/D as a function of $\sigma D^2 = (36a^2g^2\sigma)^{\frac{1}{4}}$. $E(\Sigma_0)$, which also depends on σD^2 as shown by (26), also appears in the table. Note that d_m is not just a function of a single product of powers of a, g, σ; it has a more complicated form $(ag/\sigma)^{\frac{1}{4}} \times$ function $(a^2g^2\sigma)$.

The integral in (31) is a rapidly decreasing function of d_m/D. Then the numbers in Table V would not change much if d_m were redefined with the term $\frac{1}{2}$ in (30) replaced by any other number of the same order of magnitude. For the same reason, d_m can be expected to be a good approximation to the mean range to the furthest peak.

VII. THE HORIZON

The approximation (23) will now be used to derive properties of the range from a peak P_1 to the horizon at a random azimuth angle. The range to the horizon is a more interesting random variable than the range to a random visible peak. As has been noted, it is not always clear what to count as a peak in a real landscape. But the horizon has no ambiguity.

Look from P_1 with a fixed azimuth angle. One sees only sky at high elevations and ground at low elevations. The *horizon point* is the limiting point at ground level which has the highest elevation angle. The distance z from P_1 to the horizon is the range of interest here.

Figure 11 will now be used to derive the conditions under which Q_2 is the horizon point, as seen from a peak P_1. If Q_2 is the horizon point, the entire straight line path P_1Q_2' in Fig. 11 must intersect the ground only at Q_2. Then the entire lens-shaped blocking region for Q_2' must contain no peaks. But the depth at Q_2 determines the circle on which a peak must lie. This circle appears in Fig. 11 inside the (open) blocking region. The only place that this peak can be now is on the boundary of the blocking region at one of the points of tangency T, T'.

Figure 11 shows the usual situation in which the horizon point is not on the inner sphere. There is small probability that Q_2 is on the inner sphere. In that case, q_2 is at angle $\frac{1}{2}\pi - \theta$ away from P_1, the centers c, c' coincide with q_2, and the blocking region is bounded by the circle through P_1 with center q_2. There is no second peak on the boundary of the blocking region; Q_2 lies on $M(P_1)$.

To find the probability distribution for the horizon range, one may first find the joint distribution for that range and the range r to the intersection point Q_2'. Since r is the largest range for which the corresponding blocking region is empty, the probability distribution function for r is $P(r) = 1 - \exp[-\sigma A(P_1, Q_2')]$. In this derivation, the approximation (23) will be used to write

$$P(r) = 1 - \exp[-(r/D)^3].$$

Figure 12 shows Q_2' lying at a range between r and $r + dr$, an event of probability $dP(r)$. Given this position for Q_2', the band between the boundaries of the blocking regions at r and $r + dr$ contains the peak on which the horizon point lies. The shaded part of this band is the region in which the peak must lie so that the horizon point Q_2 will have range $z_2 \leqq z$. The conditional probability function for the horizon range is just the ratio of the area of the shaded part of the band to the total area of the band. To simplify that calculation, one may replace the dotted line by a great circle that crosses P_1P_2' at right angles. That approximation leads ultimately to the conditional distribution

$$\text{Prob}\{\text{horizon range} \leqq z | r\} = (z/r)^2, \quad 0 \leqq z \leqq r. \tag{32}$$

The details are omitted because the result can almost be guessed immediately from the roughly triangular shapes of the two parts of the shaded region.

Now the unconditional probability distribution for the horizon range is obtainable from (32) by integrating

$$\begin{aligned}\text{Prob}\{\text{horizon range} \leqq z\} &= \int_0^z dP(r) + \int_z^\infty (z/r)^2 dP(r) \\ &= (z/D)^2\Gamma[\tfrac{1}{3}, (z/D)^3] + 1 - \exp[-(z/D)^3]. \end{aligned} \tag{33}$$

Table VI gives numerical values.

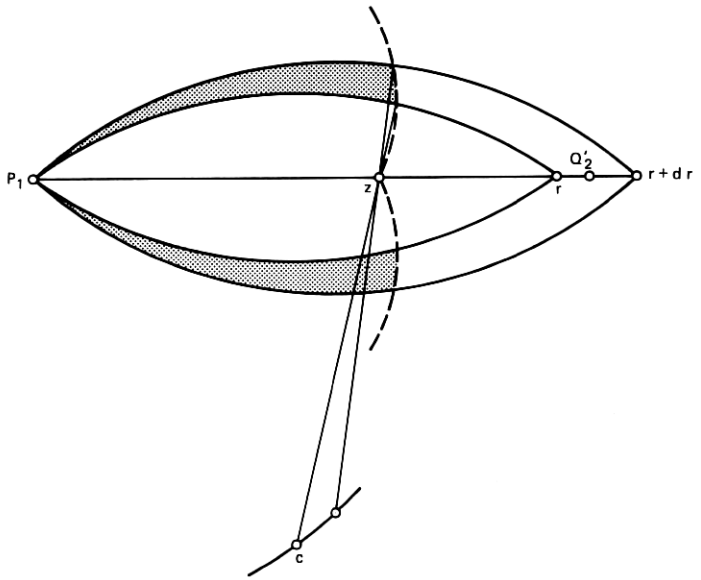

Fig. 12—Horizon at range $\leqq z$.

Table VI — Distribution function for range z to the horizon looking from peak P_1 with a random azimuth angle

z/D	Probability
0.21417	0.1
0.25	0.13625
0.35618	0.25
0.5	0.42355
0.56305	0.5
0.75	0.70432
0.79977	0.75
1.0	0.88853
1.02324	0.9
1.15749	0.95
1.25	0.97109
1.40527	0.99
1.5	0.995247
1.67110	0.999

The moments of the horizon range z are easy to find. From (33), the probability density for z is

$$2z \int_z^\infty r^{-2} dP(r).$$

The kth moment of z is

$$\begin{aligned} E(z^k) &= 2 \int_0^\infty z^{k+1} \int_z^\infty r^{-2} dP(r) dz \\ &= [2/(k+2)] E(r^k). \end{aligned}$$

The last line is obtained by integrating by parts. The expectation on the right is another integral that can be evaluated in the manner of (24) and (25). The final result is

$$E(z^k) = 2D^k \Gamma[1 + (k/3)]/(k+2). \tag{34}$$

Equation (34) with $k = 2$ is particularly interesting. If $z(\varphi)$ is the range to the horizon when looking with azimuth φ, then the mean area within horizon range is

$$\begin{aligned} E(\text{area within horizon}) &= E\left(\frac{1}{2}\int_0^{2\pi} z^2(\varphi) d\varphi\right) \\ &= \pi E(z^2) \\ &= \tfrac{1}{2}\pi \Gamma(5/3) D^2 \\ &= 1.41803 D^2. \end{aligned} \tag{35}$$

This expectation is only an upper bound on the mean area visible. For, as is clear in Fig. 4, there are points within horizon range that are obscured from view.

It is interesting to compare Tables IV and VI. At any given probability level, the range to the horizon is smaller than the range to a randomly chosen visible peak. This may be surprising at first. However, each visible peak is itself a point on the horizon. As seen in Fig. 4, the horizon consists entirely of small line segments extending down the sides of the mountains from the visible peaks. The line segments for distant peaks tend to subtend smaller azimuth angles than the segments for nearby peaks. Picking an azimuth at random, one is more likely to find the horizon point on one of the nearby visible peaks than on one far away.

Another expectation that exhibits the same effect is the mean azimuth angle between the horizon point and the peak of the mountain on which the horizon point lies. The ranges z and r determine this angle. Without belaboring the details, one can approximate this angle by its tangent and make the further approximations by which (33) was derived. The expected angle is found to be

$$\begin{aligned} E(\text{angle}) &= E[(r - z)/(2ag)] \\ &= \Gamma(4/3)D/(6ag). \end{aligned}$$

That result can be stated in a more illuminating way:

$$\begin{aligned} E(\Sigma_0)E(\text{angle}) &= \pi\Gamma(4/3)\Gamma(5/3) \\ &= (2\pi 3^{-\frac{1}{2}})(2\pi) \\ &= 0.40306(2\pi). \end{aligned}$$

By contrast, if $E(\Sigma_0)$ peaks were evenly distributed in azimuth with angular separation $2\pi/E(\Sigma_0)$, one would obtain

$$E(\Sigma_0)E(\text{angle}) = 0.25(2\pi).$$

The larger factor 0.40306 again occurs because of the variability of the angles which visible mountains subtend on the horizon.

VIII. COVERAGE AREA

The *coverage set* for a point P is the set of points Q such that a line-of-sight path PQ exists. In VHF radio applications, the coverage set of P is the set of points Q to which an antenna at P can radiate a strong signal. This section will estimate the *mean coverage area* C, the expected area of the coverage set for $P = P_1$, a peak.

The coverage set can have a very complicated shape. Figure 13 shows one coverage set. In Fig. 13, the peaks are not in a Poisson pattern; to simplify the drawing, the peaks were located at points of a regular lattice. The coverage set contains the entire mountain on which P lies plus parts of adjacent mountains. These points alone

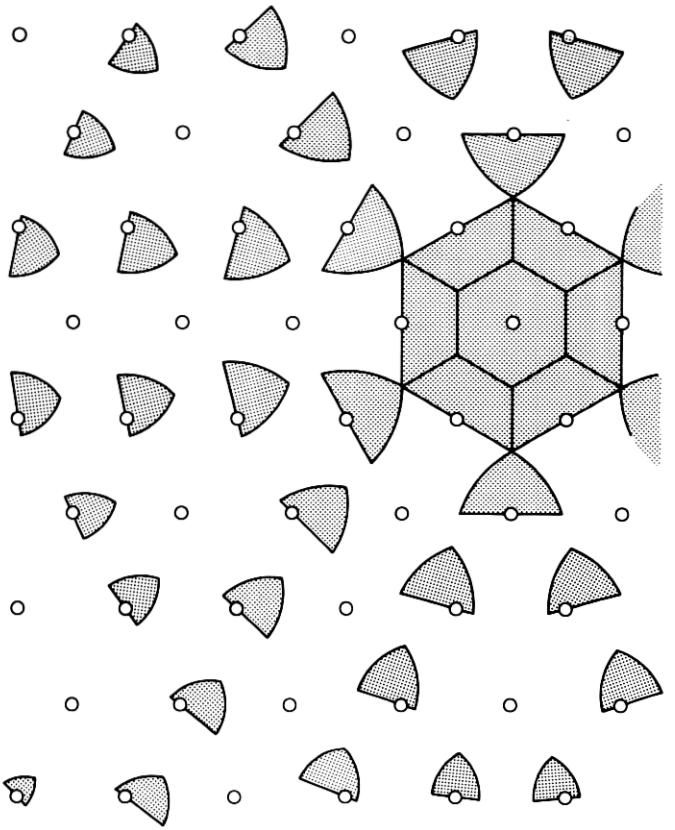

Fig. 13—A coverage set.

constitute a hexagon of area $4/\sigma$. In addition, the coverage set contains many smaller isolated patches on more remote mountains. These small patches can be so numerous that they represent most of the coverage area.

If Fig. 13 represented the coverage set of a base station in a mobile radio telephone system, the station would only serve the hexagon of area $4/\sigma$. The other small patches would lie in the service areas of other stations, and so these patches would represent places where the given station can interfere with other stations.

As in Fig. 11, let P_1 be a given peak and Q_2 another point at ground level. Suppose the distance r from P_1 to Q_2 is known, i.e., the angle $z = r/a$ in Fig. 11 is given. Let $f(r)$ denote the probability that a line-of-sight path P_1Q_2 exists. Since an element of area $dA(Q_2)$ at Q_2 belongs to the coverage set of P_1 with probability $f(r)dA(Q_2)$, the

mean area covered is

$$C = \int\int f(r)dA(Q_2) = 2\pi a^2 \int_0^{\pi} f(r) \sin z_2 dz_2. \tag{36}$$

Before attempting to evaluate $f(r)$ and C, the integral (36) will be given a second interpretation. Now consider Q_2 at a fixed location and count the number of peaks visible from Q_2. The probability that an element of area $dA(P_1)$ contains a peak P_1 visible from Q_2 is $\sigma f(r)dA(P_1)$. Then the mean number of peaks visible from Q_2 is

$$\begin{aligned} E(\text{visible peaks}) &= \sigma \int\int f(r)dA(P_1) \\ &= 2\pi a^2 \sigma \int\int f(r) \sin z_2 dz_2 \\ &= \sigma C. \end{aligned} \tag{37}$$

Equation (37) can be used to derive very simple bounds on C. Clearly, more peaks are visible from a point Q_2 at high altitudes than at low. If Q_2 were itself a peak, the mean number of visible peaks would be $E(\Sigma_0)$, given by (26). But Q_2 has probability zero of being exactly at a peak. If Q_2 is at any slightly lower altitude, Q_2 is on the side of a hill which obscures 180 degrees of the view from Q_2. Thus, $E(\text{visible peaks}) \leqq \frac{1}{2}E(\Sigma_0)$, and (37) shows

$$C \leqq E(\Sigma_0)/(2\sigma). \tag{38}$$

Curiously, the right-hand side of (38) is exactly the mean area within the horizon as given by (35). Then (38) is a bound that was obtained in Section VII.

At the other extreme, Q_2 might be on the inner sphere, where no peak is visible. In most cases, that event will be so unlikely that it will be safe to say that the worst reasonable possibility is that Q_2 is down in a valley near the point where three mountains meet. Here, the three mountain peaks are visible and so one concludes $C \geqq 3/\sigma$.

To obtain $f(r)$, and hence C, recall that (20) is a formula for the path probability $p(Q_1, Q_2)$, depending on the altitude y at Q_2. To get $f(r)$ one may average $p(Q_1, Q_2)$ over y (or γ_2). This average may be expressed as a sum of two terms which account for the possibilities that Q_2 belongs to the same mountain $M(P_1)$ as Q_1 or to a different mountain.

In Fig. 11, if $\gamma_2 = z_2$, then Q_2 lies on the mountain $M(P_1)$. This event has probability $\exp\{-2\pi\sigma a^2(1 - \cos z_2)\}$. The path probability $p(Q_1, Q_2) = 1$ if $r \leqq (\frac{1}{2}\pi - \theta)a$. If $r > (\frac{1}{2}\pi - \theta)a$, then Q_2 lies on the inner sphere, the path P_1Q_2 is blocked, and $p(Q_1, Q_2) = 0$.

If $\gamma_2 < z_2$, then Q_2 lies on a different mountain $M(P_2)$. This possibility contributes a second term to $f(r)$,

$$\int_{\gamma_2=0}^{z_2} p(Q_1, Q_2) d\{1 - \exp(-\sigma A_2)\},$$

where A_2 and $p(Q_1, Q_2)$ are given by (16) and (20).

For $r \leqq (\frac{1}{2}\pi - \theta)a$, the two terms combine into

$$f(r) = \exp\{-2\pi\sigma a^2(1 - \cos z_2)\} + \int_{\gamma_2=0}^{z_2} (1 - \varphi_2/\pi) \exp[-\sigma(A_0 + A_2)]\sigma dA_2, \quad (39)$$

where (16) and (17) provide A_2, A_0. A similar formula applies when r is larger, but $f(r)$ is very small at such large ranges.

One could find $f(r)$ to any desired accuracy by evaluating the integral in (39) numerically. Instead, (39) will be replaced by a simpler approximate formula. Since a is large, the first term of (39) is approximately $\exp(-\sigma\pi r^2)$; also, $A_2 = \pi x^2$ where $x = a\gamma_2$. The approximations to φ and A_0 which follow are not uniformly good but are intended to apply in situations that contribute most of the coverage area C. Except at very short ranges r, a typical blocking region is more elongated than that shown in Fig. 11. Figure 14 is more typical. Then $\varphi_2 = \frac{1}{2}\pi$, approximately. With that approximation, the shaded region in Fig. 14 has area $A_0 + \frac{1}{2}A_2$. It consists of a triangle, of area xr, and two extra lens-shaped pieces. The two extra pieces can fit together into one lens of exactly the shape of the blocking region for two peaks at separation r. Then the two extra pieces combined have area $r^3/(6ga)$, as in (23). Now the exponent $\sigma(A_0 + A_2)$ in (39) is approximately $(r/D)^3 + \frac{1}{2}\pi\sigma x^2$.

To substitute these approximations into (39), write

$$\begin{aligned} Y &= \sigma\pi r^2 \\ X &= r^3/(6ga) = (r/D)^3 = [\Gamma(5/3)Y/E(\Sigma_0)]^{\frac{3}{2}} \end{aligned} \quad (40)$$

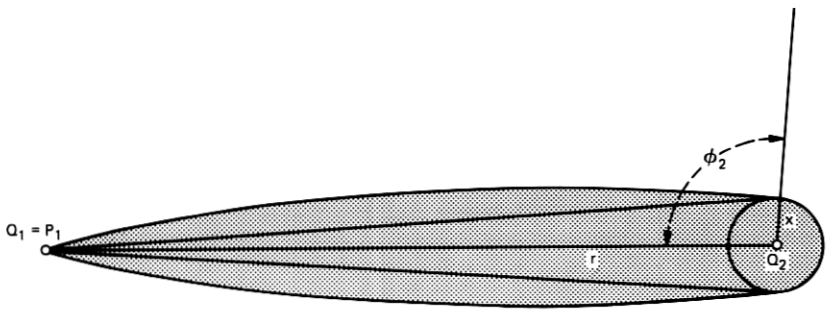

Fig. 14—Approximation of A_0 and φ_2.

and then

$$f(r) = \exp(-Y) + \pi\sigma \exp(-X) \int_0^r \exp\{-\sigma x r - \tfrac{1}{2}\sigma\pi r^2\} r dr$$

$$f(r) = \exp(-Y) + \exp(-X)\{1 - \exp(-Y[\tfrac{1}{2} + \pi^{-1}])\} + \exp(-X + \tfrac{1}{2}Y/\pi^2)(2Y/\pi)^{\frac{1}{2}} \times \{\operatorname{erf}(Y^{\frac{1}{2}}[1 + \pi^{-1}]) - \operatorname{erf}(Y^{\frac{1}{2}}/\pi)\}. \quad (41)$$

Figure 15 shows curves of $f(r)$. The ordinate $Y^{\frac{1}{2}} = (\sigma\pi)^{\frac{1}{2}}r$ was used as a convenient normalized range. It may be interpreted as the square root of the mean number of other peaks within range r of P_1. As (40) shows, the parameter $E(\Sigma_0)$ enters into $f(r)$ through the variable X. The $f(r)$ curves for different values of $E(\Sigma_0)$ lie close together at short ranges. As the range increases, $f(r)$ falls more sharply for small $E(\Sigma_0)$. There is a limiting curve, as $E(\Sigma_0) \to \infty$, which is obtained from (41) by setting $X = 0$. As (40) shows, $X = 0$ also corresponds to the limit $a \to \infty$; i.e., this limit represents the planar model.

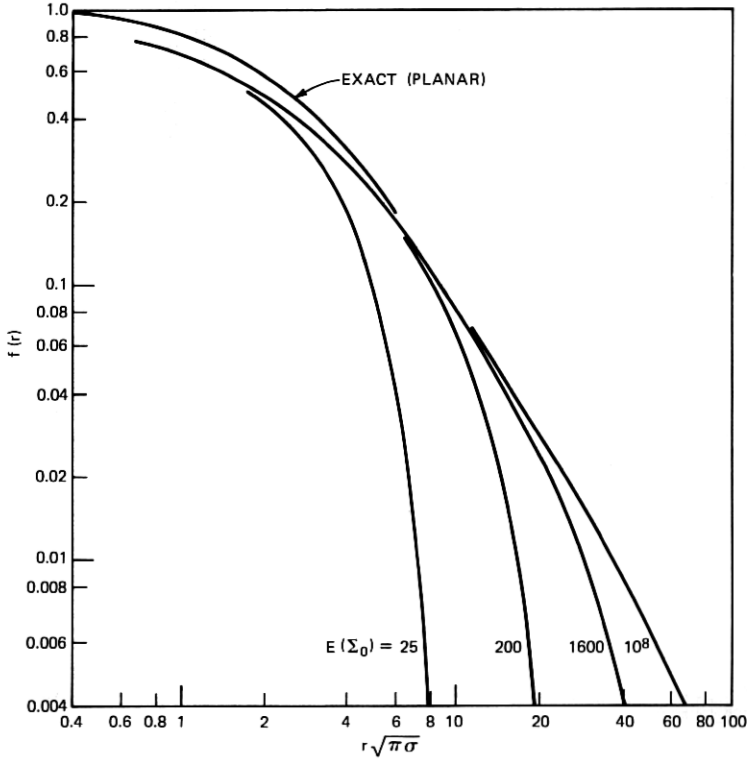

Fig. 15—Probability $f(r)$ that a random point at ground level is visible from a peak r miles away.

Table VII — Mean coverage area C

$E(\Sigma_0)$	σC
25	8.3
50	12.2
100	17.3
200	23.5
400	30.6
800	38.6
1600	47.4

The approximations which led to (41) are poor when r is small. Fortunately, the planar model is good for smaller r. The curve labeled "exact (planar)" in Fig. 15 was obtained by a numerical integration, using an exact equation (39) for the planar model. The planar curve crosses the 0.5 probability level at $Y^{\frac{1}{2}} = 2.3$. Then $r = 1.3\sigma^{-\frac{1}{2}}$ is the range at which the odds of finding a clear path are even.

The behavior of $f(r)$ for large r can be obtained by replacing the error functions in (41) by their asymptotic expansions. The leading terms are

$$f(r) \sim \exp(-Y) + \pi^2 Y^{-1} \exp(-X). \tag{42}$$

In Fig. 14, the $f(r)$ curve starts to depart from the limiting curve at values of Y near $E(\Sigma_0)$. For larger Y, the factor $\exp(-X)$ in (42) becomes small rapidly. In the planar model, $\exp(-X) = 1$ for all Y; (42) then shows that $f(r) \sim \pi^2/Y = \pi/(\sigma r^2)$.

To good approximation, the integral (36) for the mean coverage area can be replaced by

$$C = \int_0^\infty f(r)d(\pi r^2) = \sigma^{-1} \int_0^\infty f(r)dY. \tag{43}$$

The main contribution to C in (36) comes from the range $0 \leqq r \leqq (\frac{1}{2}\pi - \nu)a$, in which (39) holds exactly and (41) approximately. Then (41) will be used for $f(r)$ in (43) and, since $f(r) \to 0$ rapidly for larger r, the range of integration has been extended to $0 \leqq Y < \infty$.

Since (40) and (41) express $f(r)$ in terms of Y and the single parameter $E(\Sigma_0)$, (43) shows that σC is a function of $E(\Sigma_0)$ only. Table VII gives values of this function, obtained from (41) and (43) by numerical integration. These values also represent mean numbers of peaks visible from a random point on the ground, as (37) showed.

In Table VII, σC appears to be a slowly increasing function of $E(\Sigma_0)$. As $E(\Sigma_0) \to \infty$, the model becomes planar and then $f(r) \sim \pi^2/Y$. Then (43) shows $\sigma C \to \infty$ in the planar model limit.